

the membrane but must involve a more intricate and long-distance flow through extramembrane regions that provide opportunities for regulating channel conductance. The portals, chambers, and vestibules observed in the cytoplasmic domain MscS (Fig. 3) are reminiscent in size and organization of those described for the acetylcholine receptor (29), the Shaker potassium channel (43), and the sodium channel (44). These regions have been suggested to serve as filters that screen out impermeant molecules on the basis of size and perhaps electrostatic factors as well as to provide docking sites for other proteins to regulate conductance properties (29).

These resemblances between aspects of the structural organization and functional properties of MscS to other channels reinforce a view that the different elements of channel structure—pore, selectivity filters, sensing modules, and extramembrane domains—can be combined in various ways to create channels with distinctive properties. Over the past few years, increasing progress has been reported in defining the structural arrangements for these elements in prokaryotic channels. The immediate challenge to structural biologists now is to extend these analyses from prokaryotic channels to the more complex systems found in eukaryotes.

References and Notes

- B. Martinac, M. Buechner, A. H. Delcour, J. Adler, C. Kung, *Proc. Natl. Acad. Sci. U.S.A.* **84**, 2297 (1987).
- C. Berrier, A. Coulombe, C. Houssin, A. Ghazi, *FEBS Lett.* **259**, 27 (1989).
- B. Hille, *Ion Channels of Excitable Membranes* (Sinauer Associates, Sunderland, CT, ed. 3, 2001).
- S. I. Sukharev, P. Blount, B. Martinac, F. R. Blattner, C. Kung, *Nature* **368**, 265 (1994).
- S. Sukharev, *Biophys. J.* **83**, 290 (2002).
- C. Berrier, A. Coulombe, I. Szabo, M. Zoratti, A. Ghazi, *Eur. J. Biochem.* **206**, 559 (1992).
- S. I. Sukharev, P. Blount, B. Martinac, C. Kung, *Annu. Rev. Physiol.* **59**, 633 (1997).
- N. Levina et al., *EMBO J.* **18**, 1730 (1999).
- C. Cui, D. O. Smith, J. Adler, *J. Membr. Biol.* **144**, 31 (1995).
- D. McLaggan et al., *Mol. Microbiol.* **43**, 521 (2002).
- G. Chang, R. H. Spencer, A. T. Lee, M. T. Barclay, D. C. Rees, *Science* **282**, 2220 (1998).
- D. A. Doyle et al., *Science* **280**, 69 (1998).
- S. I. Sukharev, B. Martinac, V. Y. Arshavsky, C. Kung, *Biophys. J.* **65**, 177 (1993).
- A. Kloda, B. Martinac, *Archaea* **1**, 35 (2002).
- S. Sukharev, M. Betanzos, C.-S. Chiang, H. R. Guy, *Nature* **409**, 720 (2001).
- S. Sukharev, S. R. Durell, H. R. Guy, *Biophys. J.* **81**, 917 (2001).
- E. Perozo, A. Kloda, D. M. Cortes, B. Martinac, *Nature Struct. Biol.* **9**, 696 (2002).
- E. Perozo, D. M. Cortes, P. Sompornpisut, A. Kloda, B. Martinac, *Nature* **418**, 942 (2002).
- Y.-S. Liu, P. Sompornpisut, E. Perozo, *Nature Struct. Biol.* **8**, 883 (2001).
- Y. Jiang et al., *Nature* **417**, 515 (2002).
- Y. Jiang et al., *Nature* **417**, 523 (2002).
- F. Bezanilla, *Physiol. Rev.* **80**, 555 (2000).
- Materials and methods are available as supporting material on Science Online.
- D. C. Rees, G. Chang, R. H. Spencer, *J. Biol. Chem.* **275**, 713 (2000).
- C. Cui, J. Adler, *J. Membr. Biol.* **150**, 143 (1996).
- O. S. Smart, J. Breed, G. R. Smith, M. S. Sansom, *Biophys. J.* **72**, 1109 (1997).

- E. de la Fortelle, G. Bricogne, *Methods Enzymol.* **276**, 472 (1997).
- Collaborative Computational Project No. 4, *Acta Crystallogr.* **D50**, 760 (1994).
- T. A. Jones, J.-Y. Zou, S. W. Cowan, M. Kjeldgaard, *Acta Crystallogr.* **A47**, 110 (1991).
- A. Brünger et al., *Acta Crystallogr.* **D54**, 905 (1998).
- R. A. Laskowski, M. W. MacArthur, D. S. Moss, J. M. Thornton, *J. Appl. Crystallogr.* **26**, 283 (1993).
- P. J. Kraulis, *J. Appl. Crystallogr.* **24**, 946 (1991).
- E. A. Merritt, D. J. Bacon, *Methods Enzymol.* **277**, 505 (1997).
- O. S. Smart, J. G. Neduveilil, X. Wang, B. A. Wallace, M. S. Sansom, *J. Mol. Graph.* **14**, 354 (1996).
- A. Nicholls, K. Sharp, B. Honig, *Proteins Struct. Funct. Genet.* **11**, 281 (1991).
- A. Nicholls, B. Honig, *J. Comp. Chem.* **12**, 435 (1991).
- Supported by NIH (D.C.R.) and by a National Service Research Award postdoctoral fellowship (R.B.B.). Discussions with R. Spencer, K. Locher, A. Lee, O. Einsle, D. Dougherty, and H. Lester are greatly appreciated. We thank the staffs at the Advanced Light Source, Advanced Photon Source, National Synchrotron Light Source, and the Stanford Synchrotron Radiation Laboratory (SSRL) facilities for their invaluable assistance. These facilities are funded by the Office of Basic Energy Sciences, U.S. Department of Energy, and NIH. The coordinates have been deposited in the Protein Data Bank (1MXM) for release upon publication.

Supporting Online Material

www.sciencemag.org/cgi/content/full/298/5598/1582/DC1

Materials and Methods

Figs. S1 and S2

30 August 2002; accepted 7 October 2002

Mechanisms of AIF-Mediated Apoptotic DNA Degradation in *Caenorhabditis elegans*

Xiaochen Wang,^{1*} Chonglin Yang,^{1*} Jijie Chai,² Yigong Shi,² Ding Xue^{1†}

Apoptosis-inducing factor (AIF), a mitochondrial oxidoreductase, is released into the cytoplasm to induce cell death in response to apoptotic signals. However, the mechanisms underlying this process have not been resolved. We report that inactivation of the *Caenorhabditis elegans* AIF homolog *wah-1* by RNA interference delayed the normal progression of apoptosis and caused a defect in apoptotic DNA degradation. WAH-1 localized in *C. elegans* mitochondria and was released into the cytosol and nucleus by the BH3-domain protein EGL-1 in a caspase (CED-3)-dependent manner. In addition, WAH-1 associated and cooperated with the mitochondrial endonuclease CPS-6/endo-nuclease G (EndoG) to promote DNA degradation and apoptosis. Thus, AIF and EndoG define a single, mitochondria-initiated apoptotic DNA degradation pathway that is conserved between *C. elegans* and mammals.

Programmed cell death (apoptosis) is a fundamental feature in the development and tissue homeostasis of metazoans (1, 2). During apo-

ptosis, the cell activates a suicide machinery that executes orderly cell disassembly, including condensation and fragmentation of the chromosomal DNA (3). Many key components that initiate and execute apoptosis are conserved across species (3). For example, the onset of apoptosis is controlled by a regulatory pathway involving conserved cell death activators and inhibitors: EGL-1 and BH3-domain-only proteins, CED-9 and Bcl-2, CED-4 and Apaf-1, and CED-3 and caspases, in nematodes

¹Department of Molecular, Cellular, and Developmental Biology, University of Colorado, Boulder, CO 80309, USA. ²Department of Molecular Biology, Princeton University, Princeton, NJ 08544, USA.

*These authors contributed equally to this work.
†To whom correspondence should be addressed. E-mail: ding.xue@colorado.edu

and mammals, respectively (3). In addition, the degradation of chromosomal DNA involves a mitochondrial endonuclease: endonuclease G (EndoG) in mammals and its ortholog CPS-6 in worms (4, 5).

EndoG is one of several mitochondrial proapoptotic factors, including cytochrome c, apoptosis-inducing factor (AIF), Smac/DIABLO, and Omi/HtrA2, which are released into the cytosol to mediate various aspects of apoptosis in mammals (6–11). These factors have been proposed to act through caspase-dependent pathways (cytochrome c and Smac/DIABLO), caspase-independent pathways (AIF and EndoG), or both (Omi/HtrA2). CPS-6 is the only mitochondrial protein that has been implicated in invertebrate apoptosis (5). It is unclear whether additional mitochondrial factors regulate apoptosis in invertebrates, and if so, whether the mitochondrial cell death pathways are conserved.

AIF has been suggested to mediate caspase-independent apoptosis (12, 13). In response to apoptotic stimuli, AIF is released from mitochondria and translocated to both the cytosol and the nucleus, where it induces condensation and large-scale fragmentation of chromatin (7, 13, 14). AIF is a flavin-adenine dinucleotide (FAD)-binding oxidoreductase, but neither its FAD-binding ability nor its oxidoreductase activity is required for its apoptogenic activity (7, 15). Therefore, it is unclear how AIF induces DNA fragmentation or apoptosis. Furthermore, as an evolutionarily conserved protein (12, 15), it is unclear whether the pro-apoptotic function

of AIF is conserved in other species. To address these issues, we cloned the *C. elegans* AIF homolog *wah-1* (worm AIF homolog; GenBank accession number AY147006) and performed systematic studies to understand its biological functions, biochemical activities, and the mechanisms by which it mediates apoptosis.

WAH-1 is important for apoptosis in *C. elegans*. The sequence of the human AIF protein was used to search the *C. elegans* genome database. One putative open reading frame on linkage group III, C51G7.5, was identified, and a full-length cDNA clone corresponding to C51G7.5 was obtained with a reverse transcription-polymerase chain reaction strategy (16). The predicted 700-amino acid protein shows 37% sequence identity and 54% sequence similarity to the human AIF (fig. S1). C51G7.5 was renamed *wah-1*. Sequence similarity is particularly strong between residues 214 and 700 of WAH-1 and residues 107 and 613 of the human AIF, which correspond to the mature human AIF protein (7). The NH₂-terminal portions of the two proteins do not have sequence similarity except for the first 30 amino acids, which encode a putative mitochondrial localization sequence (fig. S1) (17). WAH-1 also shares sequence similarity to the *Dictyostelium discoideum* AIF protein (18) and a homologous protein in *Drosophila* (fig. S1).

To understand the functions of *wah-1* in *C. elegans* programmed cell death, we used RNA interference (RNAi) (19) to inhibit the expression of the *wah-1* gene in *C. elegans* (16) [these are referred to as *wah-1(RNAi)* animals]. Unlike

the situation in mice, where AIF-deficient embryonic stem cells fail to form a viable chimeric embryo (13), *wah-1(RNAi)* animals were viable but exhibited slower growth rate and a smaller brood size than wild-type animals or animals treated with an RNAi control (20). These features allowed us to examine the functions of WAH-1 in various aspects of *C. elegans* apoptosis during development.

A time-course analysis of embryonic cell corpses (5, 21) revealed that *wah-1(RNAi)* treatment delayed the appearance of embryonic cell corpses during development (Fig. 1A). The peak of cell corpses was shifted from the comma embryonic stage in wild-type animals to the twofold embryonic stage in *wah-1(RNAi)* animals ($P < 0.0001$, unpaired *t* test) (Fig. 1A). The numbers of cell corpses in later embryonic stages (2.5-fold and 3-fold) also increased in *wah-1(RNAi)* embryos ($P < 0.0001$, unpaired *t* test). This delayed corpse appearance phenotype is similar to that displayed by the *cps-6(sm116)* mutant (5). In addition, like the *cps-6(sm116)* mutation, *wah-1(RNAi)* treatment enhanced the delay-of-cell-death phenotype of the *ced-8(n1891)* mutant (21), increasing the numbers of cell corpses in fourfold stage embryos and L1 stage larvae ($P < 0.0001$, unpaired *t* test) (Fig. 1B). However, *wah-1(RNAi)* treatment did not affect the profile of corpse appearance in either the *cps-6(sm116)* mutant (Fig. 1C) or the *cps-6(sm116); ced-8(n1891)* mutant (Fig. 1D), suggesting that *wah-1* and *cps-6* may function in the same pathway to affect the progression of apoptosis.

To determine whether *wah-1(RNAi)* treat-

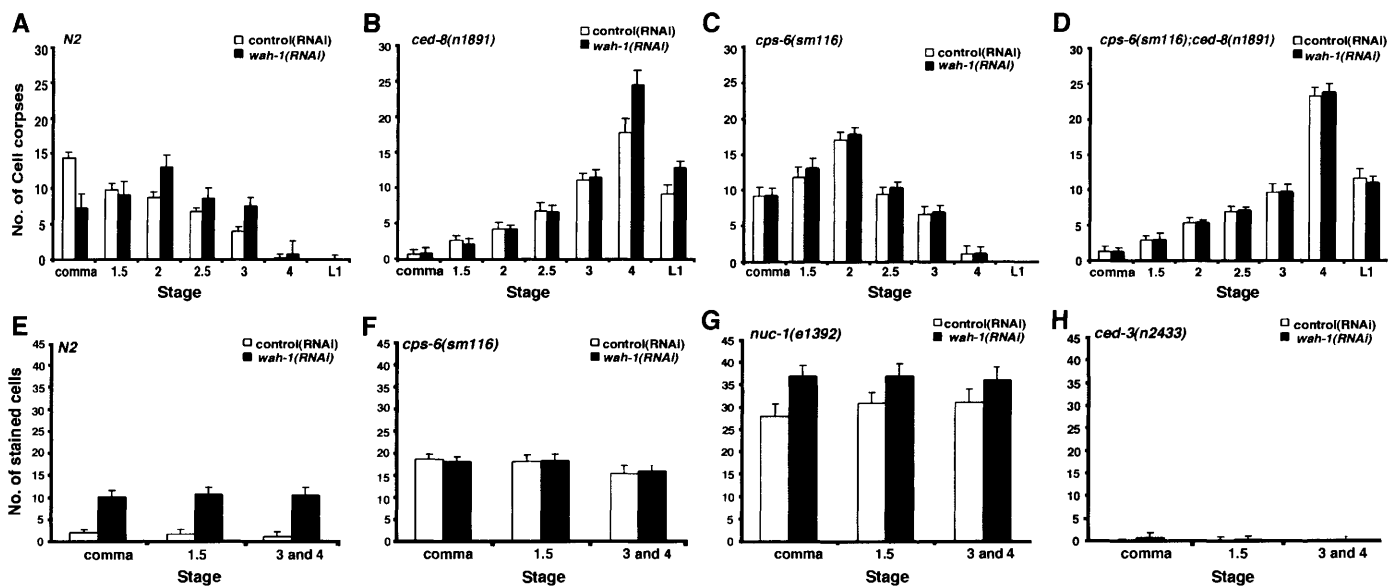


Fig. 1. *wah-1(RNAi)* affects the progression of apoptosis and apoptotic DNA degradation in *C. elegans*. L1 stage *C. elegans* larvae were treated with *wah-1(RNAi)* (filled bars) or control(RNAi) (open bars), and the progeny of the RNAi-treated animals were scored for cell corpses (A to D) or TUNEL-positive nuclei (E to H) (16). In the cell corpse assays, N2 (A), *ced-8(n1891)* (B), *cps-6(sm116)* (C), and *cps-6(sm116); ced-8(n1891)* (D) animals were scored at the following embryonic or larval

stages: comma, 1.5-fold, 2-fold, 2.5-fold, 3-fold, 4-fold, and early L1 stage larvae. In the TUNEL assays, N2 (E), *cps-6(sm116)* (F), *nuc-1(e1392)* (G), and *ced-3(n2433)* (H) animals were counted at three embryonic stages: comma, 1.5-fold, and 3- and 4-fold. The y axis represents the average number of cell corpses or TUNEL-positive nuclei scored. Error bars indicate SEM. At least 15 animals were scored for each developmental stage in each assay.

ment could prevent cell death, we examined cells in the anterior pharynx of treated animals (21). Treatment with *wah-1(RNAi)* alone had little effect on the deaths of the 16

cells in this region that normally undergo apoptosis (Table 1). However, *wah-1(RNAi)* treatment enhanced the cell survival phenotypes of mutants that are partially defective in

apoptosis, such as animals that are homozygous for a partial loss-of-function mutation in the *ced-3* gene (*n2438* or *n2447*) or the *ced-4* gene (*n2273*) (Table 1). For instance, in *ced-3(n2447)* animals, an average of 1.2 extra cells was seen in the anterior pharynx, compared with a mean of 2.7 extra cells observed in *ced-3(n2447); wah-1(RNAi)* animals ($P < 0.003$, unpaired *t* test) (Table 1). Treatment with *wah-1(RNAi)* also enhanced the cell survival phenotypes of mutants that are strongly defective in cell death, such as *ced-3(n2433)* or *ced-4(n1162)* ($P < 0.02$, unpaired *t* test) (Table 1). These data suggest that *wah-1*, like the *cps-6* gene, not only is important for the normal progression of apoptosis but also can promote cell killing.

WAH-1 promotes apoptotic DNA degradation. Because human AIF induces large-scale chromosome fragmentation (7), we examined apoptotic DNA degradation in nematodes treated with *wah-1(RNAi)* using TUNEL (terminal deoxynucleotidyl transferase-mediated dUTP nick-end labeling) assay (22). Wild-type *C. elegans* embryos treated with *wah-1(RNAi)* contained more TUNEL-positive nuclei than did control embryos at several embryonic stages examined (Fig. 1E), suggesting that WAH-1 is involved in resolving the TUNEL-positive DNA breaks. The numbers of TUNEL-positive nuclei observed in *wah-1(RNAi)* embryos were lower than those observed in the *cps-6(sm116)* mutant (5) or a mutant (*e1392*) defective in the *nuc-1* gene, which encodes a deoxyribonuclease II homolog and has been implicated in mediating apoptotic DNA degradation in *C. elegans* (22) (Fig. 1, F and G). The TUNEL-positive nuclei found in *wah-1(RNAi)* embryos likely represent cells undergoing apoptosis, because the *ced-3(n2433)* mutation that blocks almost all cell death in nematodes abolished the TUNEL staining in *wah-1(RNAi)* embryos (Fig. 1H).

Similar numbers of TUNEL-positive cells were observed in *cps-6(sm116); wah-1(RNAi)* embryos or control *cps-6(sm116)* embryos; however, *nuc-1(e1392); wah-1(RNAi)* embryos had higher numbers of TUNEL-positive nuclei than did control *nuc-1(e1392)* embryos or *wah-1(RNAi)* embryos ($P < 0.0001$, unpaired *t* test) (Fig. 1, F and G). These results suggest that *wah-1* and *cps-6* likely function in the same DNA degradation pathway, consistent with observations that *wah-1(RNAi)* does not enhance the cell death defects of the *cps-6(sm116)* mutant (Fig. 1, C and D). In contrast, *nuc-1* appears to be dispensable for apoptosis (5, 22, 23) and likely functions in a different DNA degradation process.

WAH-1 localizes to mitochondria and can be released by EGL-1. To examine the subcellular localization of WAH-1, we expressed a fusion protein composed of WAH-1 and green fluorescent protein (WAH-1::GFP)

Table 1. *wah-1(RNAi)* enhances the cell death defects of the *ced-3* and *ced-4* mutants. RNAi experiments were carried out with a bacterial feeding protocol (16). "Control(RNAi)" indicates that the animals were fed bacteria containing an expression vector without an insert as a negative control. Extra cells were counted in the anterior pharynx of L4 hermaphrodites using Nomarski optics (16); the data are shown as means \pm SEM.

Strain	Number scored	Number of extra cells	Range
N2; control(RNAi)	26	0.00 \pm 0.00	0
N2; <i>wah-1(RNAi)</i>	26	0.04 \pm 0.20	0 to 1
<i>cps-6(sm116)</i> ; control(RNAi)	24	0.04 \pm 0.20	0 to 1
<i>cps-6(sm116)</i> ; <i>wah-1(RNAi)</i>	26	0.12 \pm 0.33	0 to 1
<i>ced-3(n2447)</i> ; control(RNAi)	18	1.22 \pm 1.26	0 to 4
<i>ced-3(n2447)</i> ; <i>wah-1(RNAi)</i>	17	2.71 \pm 1.40	1 to 6
<i>ced-3(n2438)</i> ; control(RNAi)	23	1.57 \pm 0.99	0 to 4
<i>ced-3(n2438)</i> ; <i>wah-1(RNAi)</i>	26	2.77 \pm 1.39	0 to 5
<i>ced-3(n2433)</i> ; control(RNAi)	24	13.7 \pm 1.46	11 to 16
<i>ced-3(n2433)</i> ; <i>wah-1(RNAi)</i>	25	14.7 \pm 1.46	12 to 16
<i>ced-4(n2273)</i> ; control(RNAi)	28	2.61 \pm 1.59	1 to 7
<i>ced-4(n2273)</i> ; <i>wah-1(RNAi)</i>	30	3.97 \pm 1.30	2 to 7
<i>ced-4(n1162)</i> ; control(RNAi)	20	13.4 \pm 1.63	11 to 16
<i>ced-4(n1162)</i> ; <i>wah-1(RNAi)</i>	24	14.6 \pm 1.53	12 to 16

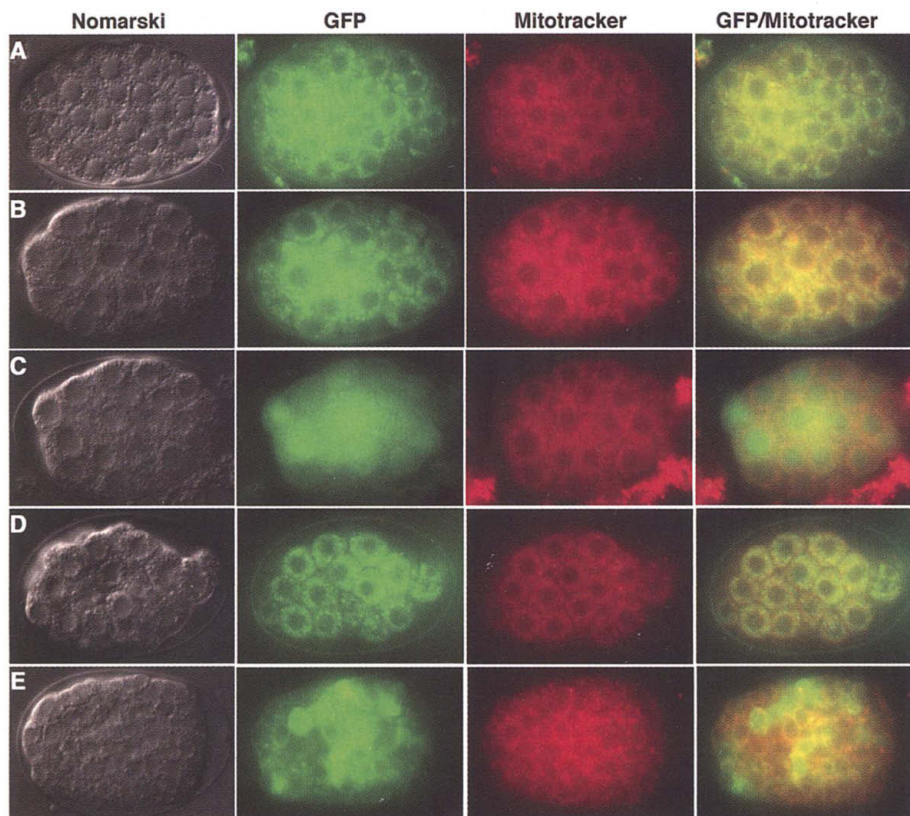


Fig. 2. WAH-1 localizes to mitochondria and can be released by EGL-1. The Nomarski, GFP, and Mitotracker Red images and the merged image of GFP and Mitotracker Red (from left to right) of an early *C. elegans* embryo from the following strains are shown: N2 animal transgenic for $P_{wah-1}::wah-1::gfp$ (A); *ced-1(e1735); egl-1(n3082)* animal transgenic for both $P_{wah-1}::wah-1::gfp$ and $P_{hsp}::egl-1$ constructs without heat-shock treatment (B) or after heat-shock treatment at 33°C for 1 hour (C) (16); *ced-1(e1735); ced-3(n2433); egl-1(n3082)* animal transgenic for both $P_{wah-1}::wah-1::gfp$ and $P_{hsp}::egl-1$ after heat-shock treatment at 33°C for 1 hour (D and E) (16). WAH-1::GFP was not released from mitochondria in the embryo shown in (D) but was partially released in the embryo shown in (E).

under the control of the *wah-1* promoter ($P_{wah-1}::wah-1::gfp$) (16). WAH-1::GFP was widely expressed in embryos and larvae (Fig. 2) (20), displaying a punctate, cytoplasmic staining pattern similar to the mitochondrial localization pattern of CPS-6 (5) (Fig. 2A). The staining pattern of WAH-1::GFP coincided with that of Mitotracker Red, a mitochondria-specific fluorescent dye (24), confirming that WAH-1 localized within mitochondria (Fig. 2A).

In mammals, the BH3-domain-only proteins such as Bid and Bim can cause release of mitochondrial apoptogenic factors in response to apoptotic signals (4, 25–28). However, it is unclear whether a similar mitochondrial cell death pathway exists in *C. elegans*. Because the *C. elegans* BH3-domain protein EGL-1 is thought to be the most upstream cell death activator that receives and integrates cell death stimuli (29, 30), we determined whether induction of global expression of EGL-1 under the control of the *C. elegans* heat-shock promoters ($P_{hsp}::egl-1$) could cause the release of WAH-1 from mitochondria. Upon heat-shock treatment of *egl-1(n3082)* embryos transgenic for both $P_{wah-1}::wah-1::gfp$ and $P_{hsp}::egl-1$, WAH-1::GFP lost its normally punctate, cytoplasmic staining pattern (Fig. 2B) and, instead, adopted a more uniform localization pattern with more intense GFP fluorescence seen in the nuclei (Fig. 2C). This result indicates that WAH-1 was released from mitochondria and translocated to nuclei by EGL-1 and that a mitochondrial cell death pathway similar to the one used in mammals likely exists in *C. elegans*.

In mammals, AIF appears to mediate a caspase-independent cell death pathway (7, 13). We thus examined whether the CED-3 caspase activity in nematodes is dispensable for the release of WAH-1 from the mitochondria. Expression of EGL-1 in *ced-3(n2433); egl-1(n3082)* embryos transgenic for both $P_{wah-1}::wah-1::gfp$ and $P_{hsp}::egl-1$ failed to induce the release of WAH-1 in most of the embryos (Fig. 2D). In 17% of the embryos ($n = 197$), WAH-1::GFP was observed in ~10% of the nuclei, indicating partial release of WAH-1 (Fig. 2E). In contrast, WAH-1::GFP was completely released from mitochondria by EGL-1 in 98% of *egl-1(n3082)* embryos ($n = 50$). Time-course analysis indicated that the reduction or block of the WAH-1 release in *ced-3(n2433); egl-1(n3082)* embryos was not due to a delay in the mitochondrial release of WAH-1 (20). These observations suggest that the CED-3 caspase activity is important for the proper release of WAH-1 during apoptosis and that WAH-1 acts in a caspase-dependent manner in *C. elegans*.

WAH-1 cooperates with CPS-6 to promote DNA degradation. To better understand how WAH-1 affects apoptosis in *C. elegans*, we performed biochemical characterization of WAH-1. When human AIF is imported into mitochondria from the cyto-

plasm, it is cleaved after residue 101 to generate a mature protein (7). WAH-1 is likely to be processed similarly in *C. elegans*. We thus generated and purified a truncated form of WAH-1, WAH-1(196–700), which contains the region most homologous to the mature human AIF protein (fig. S1). Intriguingly, the recombinant WAH-1(196–700) protein was completely colorless (31), and absorption spectrum analysis showed that it lacked the critical cofactor FAD required for typical oxidoreductases (fig. S2) (16, 31).

Because *wah-1* and *cps-6* appear to function in the same apoptotic DNA degradation pathway (Fig. 1), we tested whether WAH-1 interacts with CPS-6, using a glutathione *S*-transferase (GST) fusion protein pull-down

assay. Purified, histidine-tagged WAH-1 protein [WAH-1(196–700)-His₆] interacted with a GST–CPS-6 fusion protein that was immobilized on glutathione Sepharose beads, but not with the GST protein (Fig. 3A). In contrast, an unrelated human protein, CDC34-His₆, did not associate with the GST–CPS-6 protein in the pull-down assay (Fig. 3A), indicating that WAH-1 interacted specifically with CPS-6.

We tested whether WAH-1 interacts with CPS-6 to promote DNA degradation, using a plasmid cleavage assay (4). A low concentration (0.5 ng/μl) of CPS-6 caused nicking of a plasmid DNA substrate, converting the supercoiled DNA into open circle forms (Fig. 3B). At higher concentrations (>5 ng/μl), CPS-6

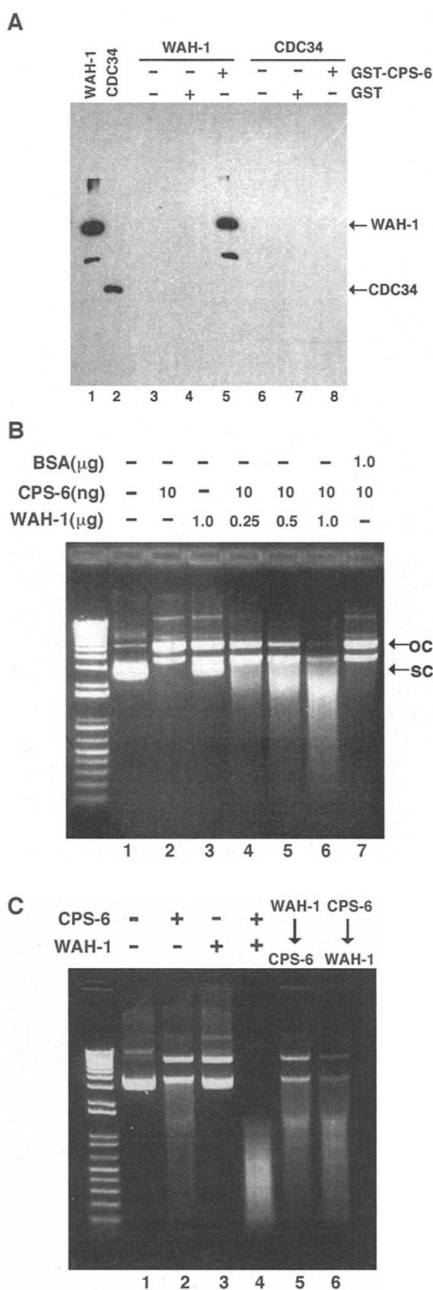


Fig. 3. WAH-1 cooperates with CPS-6 to promote DNA degradation. **(A)** WAH-1 associates with CPS-6 in vitro. Purified GST or GST–CPS-6 (1 μg each) immobilized on glutathione-Sepharose beads was incubated with similar amounts of WAH-1(196–700)-His₆ or CDC34-His₆ at room temperature for 2 hours (16). The beads were washed extensively. The bound proteins were resolved on a 10% SDS-polyacrylamide gel, transferred to a nitrocellulose membrane, and visualized by Western analysis with antibody to His₆. **(B)** WAH-1 cooperates with CPS-6 to degrade DNA. Plasmid (1 μg) was incubated with buffer alone (lane 1), with indicated amounts of CPS-6 or WAH-1(196–700), or with both at 37°C for 1 hour before the reactions were resolved on a 1% agarose gel (16). Supercoiled (sc) and open circle (oc) forms of plasmid are indicated. **(C)** WAH-1 and CPS-6 need to act together to promote DNA degradation. Plasmid (1 μg) was incubated in buffer alone (lane 1), with 20 ng of His₆CPS-6(22–308) (lanes 2 and 6), with 1 μg of WAH-1(196–700)-His₆ (lanes 3 and 5), or with 20 ng of His₆CPS-6(22–308) and 1 μg of WAH-1(196–700)-His₆ (lane 4) at 37°C for 30 min. The reactions in lanes 1 to 4 were stopped by freezing. The reactions shown in lanes 5 and 6 were passed through mini Ni²⁺-nitrilotriacetic acid columns to remove the His₆-tagged proteins. Twenty nanograms of His₆CPS-6(22–308) (lane 5) or 1 μg of WAH-1(196–700)-His₆ (lane 6) was then added into the flow-through, and the reactions were incubated for an additional 30 min at 37°C before they were resolved on a 1% agarose gel together with the products from lanes 1 to 4.

further cleaved the plasmid DNA into smaller DNA fragments, yielding a smear pattern of degradation products (5). In contrast, the recombinant WAH-1(196–700) protein does not degrade DNA, even at a high concentration (50 ng/ μ l) (Fig. 3B) (20). However, when both CPS-6 and WAH-1 were incubated with the plasmid DNA at concentrations where neither protein alone exhibited significant nuclease activity, WAH-1(196–700) cooperated with CPS-6 to efficiently degrade DNA in a concentration-dependent manner (Fig. 3B), generating progressively smaller DNA fragments. This result suggests that WAH-1 and CPS-6 cooperate to promote DNA degradation.

To rule out the possibility that WAH-1 and CPS-6 act independently but in a sequential manner to promote DNA degradation, we incubated WAH-1(196–700)-His₆ with plasmid DNA for a fixed amount of time and then depleted it from the reaction before His₆CPS-6(22–308) was added to the reaction (Fig. 3C). We performed a similar experiment in which the incubation order of these two proteins was reversed (Fig. 3C). In both cases, the extent of DNA degradation was far less severe than that observed when WAH-1 and CPS-6 were incubated together with the DNA substrate (Fig. 3C), indicating that WAH-1 and CPS-6 need to be present simultaneously to promote efficient DNA degradation, possibly through protein-protein interaction. Together, these results demonstrate that WAH-1 and CPS-6, two mitochondrial proteins, associate and cooperate to promote DNA degradation and likely function in the same apoptotic DNA degradation pathway as that observed in vivo.

WAH-1 synergizes with CPS-6 to induce cell killing. Because WAH-1 and CPS-6 can

interact in vitro to promote DNA degradation, we determined whether they could cooperate in vivo to promote cell killing. To assess the killing activity of WAH-1 and CPS-6, we ectopically expressed one or both proteins in six touch receptor neurons under the control of the *C. elegans mec-7* promoter (32) and then scored the percentage of PLM touch receptor neurons that were killed. When expressed individually in the touch cells, WAH-1(214–700), which lacks the mitochondrial targeting sequence, or full-length CPS-6 had a marginal killing activity, resulting in the death of ~5 to 8% or ~15 to 23% of the PLM neurons, respectively (Table 2). In contrast, when WAH-1(214–700) and CPS-6 were coexpressed in touch cells, ~53 to 75% of PLM neurons were killed, suggesting that WAH-1 and CPS-6 can synergize to induce cell killing (Table 2). The ectopic cell killing induced by WAH-1/CPS-6 was significantly inhibited by the strong loss-of-function *ced-3(n2433)* mutation (Table 2), indicating that WAH-1/CPS-6 induced cell killing partially through *ced-3*. These results further support the conclusion that *wah-1* and *cps-6* cooperate to promote apoptotic DNA degradation and apoptosis.

AIF and EndoG define a single conserved DNA degradation pathway. As a FAD-binding oxidoreductase, mammalian AIF induces apoptosis independently of its oxidoreductase activity (7, 15). Our finding that the recombinant WAH-1 protein can promote DNA degradation in the absence of FAD further supports the generality of this conclusion. It has been suggested that AIF may exert its functions by interacting with

downstream effectors (7, 13). Our observations that WAH-1 associated and cooperated with CPS-6 to promote DNA degradation in vitro, that *wah-1(RNAi)* animals and *cps-6* mutants display similar cell death and DNA degradation defects, and that both WAH-1 and CPS-6 localized to the mitochondria (5) and synergized to induce cell killing indicate that CPS-6/EndoG is an important nuclease target or effector that WAH-1/AIF interacts with to promote apoptotic DNA degradation. Thus, EndoG and AIF appear to define a single conserved DNA degradation pathway initiated from the mitochondria.

AIF and EndoG are two of the expanding list of apoptogenic proteins that are released from mitochondria to promote apoptosis in mammals (6–11, 28). In invertebrates, the evidence for an important role of mitochondria in apoptosis has not been strong (3, 5, 33). In our studies, we showed that WAH-1, a *C. elegans* mitochondrial apoptogenic factor, can be released by the BH3 domain-only protein EGL-1 into the cytosol and the nucleus in a manner similar to the release of cytochrome c or EndoG from mammalian mitochondria by the BH3-domain proteins (4, 25–27). This finding strongly suggests that the mitochondrial cell death pathway is evolutionarily conserved.

It is somewhat surprising that the release of WAH-1 from mitochondria in *C. elegans* partially depends on the activity of the CED-3 caspase, in contrast to the observation that the release of mammalian AIF is caspase independent (12, 13). It is likely that the initial, limited release of WAH-1 may be CED-3 independent, whereas the complete release of WAH-1 depends on the activation of the CED-3 caspase, which could amplify the damage to mitochondria by cleaving downstream CED-3 targets and promote further release of WAH-1. Our studies of AIF-mediated apoptosis in *C. elegans* indicate that different cell death pathways interact and likely cross-regulate one another in the process to activate the entire apoptotic program.

Table 2. WAH-1 and CPS-6 synergize to promote cell killing. In the P_{mec-7} -WAH-1 Δ N construct, WAH-1(214–700) was expressed under the control of the *mec-7* promoter. In P_{mec-7} -CPS-6, the full-length CPS-6 protein was expressed. The indicated transgene construct (50 μ g/ml each) was injected into *bzIs8* or *ced-3(n2433)*; *bzIs8* animals with pRF4 (50 μ g/ml), a dominant coinjection marker (34). *bzIs8* is an integrated transgenic array containing P_{mec-7} -*gfp*, which directs GFP expression in six touch receptor neurons and allows scoring of the PLM neurons. Each numbered array represents an independent transgenic line. The percentage of surviving PLM neurons was scored in the L4 larval stage animals with a fluorescent Nomarski microscope. Thirty Roller transgenic animals were counted for each transgenic line. In *bzIs8* or *ced-3(n2433)*; *bzIs8* animals, 100% of PLM neurons survived.

Transgene	Array	PLM surviving (%)
P_{mec-7} -WAH-1 Δ N	1	95
	2	92
	3	93
P_{mec-7} -CPS-6	1	85
	2	77
P_{mec-7} -WAH-1 Δ N/ P_{mec-7} -CPS-6	1	47
	2	25
	3	35
<i>ced-3(n2433)</i> ; P_{mec-7} -WAH-1 Δ N	1	92
	2	93
	3	98
<i>ced-3(n2433)</i> ; P_{mec-7} -CPS-6	1	83
	2	82
<i>ced-3(n2433)</i> ; P_{mec-7} -WAH-1 Δ N/ P_{mec-7} -CPS-6	1	78
	2	70
	3	68

References and Notes

1. H. Steller, *Science* **267**, 1445 (1995).
2. D. L. Vaux, S. J. Korsmeyer, *Cell* **96**, 245 (1999).
3. H. R. Horvitz, *Cancer Res.* **59**, 1701 (1999).
4. L. Y. Li, X. Luo, X. Wang, *Nature* **412**, 95 (2001).
5. J. Parrish et al., *Nature* **412**, 90 (2001).
6. X. Liu, C. N. Kim, J. Yang, R. Jemmerson, X. Wang, *Cell* **86**, 147 (1996).
7. S. A. Susin et al., *Nature* **397**, 441 (1999).
8. C. Du, M. Fang, Y. Li, L. Li, X. Wang, *Cell* **102**, 33 (2000).
9. A. Verhagen et al., *Cell* **102**, 43 (2000).
10. Y. Suzuki et al., *Mol. Cell* **8**, 613 (2001).
11. R. Hegde et al., *J. Biol. Chem.* **277**, 432 (2002).
12. E. Daugas et al., *FEBS Lett.* **476**, 118 (2000).
13. N. Joza et al., *Nature* **410**, 549 (2001).
14. M. Loeffler et al., *FASEB J.* **15**, 758 (2001).
15. M. D. Miramar et al., *J. Biol. Chem.* **276**, 16391 (2001).
16. Materials and Methods are available as supporting material on Science Online.
17. M. G. Claros, P. Vincens, *Eur. J. Biochem.* **241**, 779 (1996).

18. D. Arnoult *et al.*, *Mol. Biol. Cell* **12**, 3016 (2001).
 19. A. Fire *et al.*, *Nature* **391**, 806 (1998).
 20. X. Wang, C. Yang, D. Xue, unpublished results.
 21. G. M. Stanfield, H. R. Horvitz, *Mol. Cell* **5**, 423 (2000).
 22. Y. C. Wu, G. M. Stanfield, H. R. Horvitz, *Genes Dev.* **14**, 536 (2000).
 23. E. M. Hedgecock, J. E. Sulston, J. N. Thomson, *Science* **220**, 1277 (1983).
 24. F. Chen *et al.*, *Science* **287**, 1485 (2000).
 25. H. Li, H. Zhu, C. J. Xu, J. Yuan, *Cell* **94**, 491 (1998).
 26. X. Luo, I. Budihardjo, H. Zou, C. Slaughter, X. Wang, *Cell* **94**, 481 (1998).
 27. A. Gross *et al.*, *J. Biol. Chem.* **274**, 1156 (1999).
 28. X. Wang, *Genes Dev.* **15**, 2922 (2001).
 29. B. Conradt, H. R. Horvitz, *Cell* **93**, 519 (1998).
 30. ———, *Cell* **98**, 317 (1999).
 31. J. Cai, Y. Shi, unpublished results.
 32. C. Savage *et al.*, *J. Cell Sci.* **107**, 2165 (1994).
 33. Z. Song, H. Steller, *Trends Cell Biol.* **9**, M49 (1999).
 34. C. C. Mello, J. M. Krame, D. Stinchcomb, V. Ambros, *EMBO J.* **10**, 3959 (1992).
 35. We thank A. Fire, Y. Kohara, and M. Driscoll for reagents and strains; J. Parrish for discussion; and Y. C. Wu, B. Boswell, and X. D. Liu for helpful comments on this

manuscript. This work was supported in part by Searle Scholar Awards (D.X. and Y.S.), a Rita Allen Scholar Award (Y.S.), the Burroughs Wellcome Fund Career Award (D.X.), and grants from the U.S. Department of Defense (D.X.) and NIH (D.X. and Y.S.).

Supporting Online Material

www.sciencemag.org/cgi/content/full/298/5598/1587/DC1

Materials and Methods
References and Notes
Figs. S1 and S2

16 July 2002; accepted 27 September 2002

Determination of the Equation of State of Dense Matter

Paweł Danielewicz,^{1,2} Roy Lacey,³ William G. Lynch^{1*}

Nuclear collisions can compress nuclear matter to densities achieved within neutron stars and within core-collapse supernovae. These dense states of matter exist momentarily before expanding. We analyzed the flow of matter to extract pressures in excess of 10^{34} pascals, the highest recorded under laboratory-controlled conditions. Using these analyses, we rule out strongly repulsive nuclear equations of state from relativistic mean field theory and weakly repulsive equations of state with phase transitions at densities less than three times that of stable nuclei, but not equations of state softened at higher densities because of a transformation to quark matter.

The nucleon-nucleon interaction is generally attractive at nucleon-nucleon separations of $(r) = 1$ to 2 fm (1×10^{-13} cm to 2×10^{-13} cm) but becomes repulsive at small separations (< 0.5 fm), making nuclear matter difficult to compress. As a consequence, most stable nuclei are at approximately the same “saturation” density, $\rho_0 \approx 2.7 \times 10^{14}$ g/cm³, in their interiors, and higher densities do not occur naturally on Earth. Matter at densities of up to $\rho = 9 \rho_0$ may be present in the interiors of neutron stars (1), and matter at densities up to about $\rho = 4 \rho_0$ may be present in the core collapse of type II supernovae (2). The relationship between pressure, density, and temperature described by the equation of state (EOS) of dense matter governs the compression achieved in supernovae and neutron stars, as well as their internal structure and many other basic properties (1–5). Models that extrapolate the EOS from the properties of nuclei near their normal density and from nucleon-nucleon scattering are commonly exploited to study such dense systems (1, 3–9). Consequently, it is important to test these extrapolations with laboratory measurements of high-density matter.

Nuclear collisions provide the only means to compress nuclear matter to high density within a laboratory environment. The pressures that result from the high densities achieved during such collisions strongly influence the motion of ejected matter and provide the sensitivity to the EOS that is needed for its determination (10–19). Full equilibrium is often not achieved in nuclear collisions. Therefore, it is necessary to study experimental observables that are associated with the motions of the ejected matter and to describe them theoretically with a dynamical theory (20–27).

To relate the experimental observables to the EOS and the other microscopic sources of pressure, we apply a model formulated within relativistic Landau theory, which includes both stable and excited (Δ , N^*) nucleons (that is, baryons) as well as pions (20, 28). It describes the motion of these particles by predicting the time evolution of the (Wigner) one-body phase space distribution functions $f(\mathbf{r}, \mathbf{p}, t)$ for these particles, using a set of Boltzmann equations of the form

$$\frac{\partial f}{\partial t} + (\nabla_{\mathbf{p}} \varepsilon) \times (\nabla_{\mathbf{r}} f) - (\nabla_{\mathbf{r}} \varepsilon) \times (\nabla_{\mathbf{p}} f) = I \quad (1)$$

In this expression, $f(\mathbf{r}, \mathbf{p}, t)$ can be viewed semi-classically as the probability of finding a particle, at time t , with momentum \mathbf{p} at position \mathbf{r} . The single-particle energies ε in Eq. 1 are given in a local frame by

$$\varepsilon = KE + U \quad (2)$$

where KE is the kinetic energy and U is the average (mean field) potential, which depends on the position and the momentum of the particle and is computed self-consistently using the distribution functions $f(\mathbf{r}, \mathbf{p}, t)$ that satisfy Eq. 1 (20, 28). The particle density is $\rho(\mathbf{r}, t) = \int d\mathbf{p} \times f(\mathbf{r}, \mathbf{p}, t)$; the energy density e can be similarly computed from ε and $f(\mathbf{r}, \mathbf{p}, t)$ by carefully avoiding an overcounting of potential energy contributions.

The collision integral I on the right-hand side of Eq. 1 governs the modifications of $f(\mathbf{r}, \mathbf{p}, t)$ by elastic and inelastic two-body collisions caused by short-range residual interactions (20, 28). The motions of particles reflect a complex interplay between such collisions and the density and momentum dependence of the mean fields. Experimental measurements (12–19, 29–31), theoretical innovations, and detailed analyses (10, 20–29, 32–34) have all provided important insights into the sensitivity of various observables to two-body collisions (29, 32) and the density and momentum dependence (28, 33, 34) of the mean fields. The present work builds on these earlier pioneering efforts.

Compression and expansion dynamics in energetic nucleus-nucleus collisions.

Collision dynamics play an important role in studies of the EOS. Several aspects of these dynamics are illustrated in Fig. 1 for a collision between two Au nuclei at an incident kinetic energy of 2 GeV per nucleon (394 GeV). The observables sensitive to the EOS are chiefly related to the flow of particles from the high-density region in directions perpendicular (transverse) to the beam axis. This flow is initially zero but grows with time as the density grows and pressure gradients develop in directions transverse to the beam axis. The pressure can be calculated in the equilibrium limit by taking the partial derivative of the energy density e with respect to the baryon (primarily nucleon) density ρ

$$P = \rho^2 \times \left(\frac{\partial(e/\rho)}{\partial \rho} \right) \Big|_{s/\rho} \quad (3)$$

at constant entropy per nucleon s/ρ in the colliding system. The pressure developed in the simulated collisions (Fig. 1) is computed microscopically from the pressure-stress tensor $T^{\mathbf{ij}}$, which is the nonequilibrium analog of the pressure [see supporting online material

¹National Superconducting Cyclotron Laboratory and Department of Physics and Astronomy, Michigan State University, East Lansing, MI 48824–1321, USA.

²Gesellschaft für Schwerionenforschung, 64291 Darmstadt, Germany. ³Department of Chemistry, State University of New York, Stony Brook, NY 11794–3400, USA.

*To whom correspondence should be addressed. E-mail: lynch@nscl.msu.edu